Frontiers in Bioscience Landmark

Front. Biosci. (Landmark Ed) **2026**; 31(7): 51233
https://doi.org/10.31083/FBL51233

Original Research

GSDMB as a Therapeutic and Prognostic Target in Clear Cell Renal Cell Carcinoma: Insights From Pyroptosis-Related Gene Analysis

Guijiao Li[1,†], Yuerong Li[1,†], Wu Xu[1,2], Lingfei Yan[1], Qi Xiang[1], Yang Luo[1], Yufeng Liu[1], Qing Li[1], Cuilian Li[1,*], Tao Wang[1,*]

[1]Department of Urology, The Fifth Affiliated Hospital, Southern Medical University, 510900 Guangzhou, Guangdong, China
[2]Medical Research Institute, Guangdong Provincial People's Hospital, Guangdong Academy of Medical Sciences, Southern Medical University, 510900 Guangzhou, Guangdong, China
*Correspondence: 2422147657@qq.com (Cuilian Li); smu02204633@i.smu.edu.cn (Tao Wang)
†These authors contributed equally.
Academic Editor: Graham Pawelec
Submitted: 25 February 2026 Revised: 13 May 2026 Accepted: 29 May 2026 Published: 17 July 2026

Abstract

Background: Recent research has identified pyroptosis as a distinct form of programmed cell death that is strongly correlated with tumor outcomes. However, its value as a prognostic biomarker in clear cell renal cell carcinoma (ccRCC) is not yet fully established. **Methods:** Differential expression of pyroptosis-related genes between ccRCC and normal tissues was identified using the DESeq2 R package. Next, univariate and least absolute shrinkage and selection operator (LASSO) Cox regression analyses using data from The Cancer Genome Atlas cohort were applied to develop a prognostic model. Univariate and multivariate prognostic analyses were conducted to determine whether the risk score could independently predicted patient prognosis after adjustment for clinicopathological characteristics. A nomogram was then constructed to estimate patient survival probability, supporting clinical decision-making. Expression of pyroptosis-related proteins was assessed using tissue proteomic data from the Clinical Proteomic Tumor Analysis Consortium (CPTAC) database. Additionally, the Tumor-Immune System Interaction Database (TISIDB) database was used to analyze immune cell infiltration, whereas gasdermin B (GSDMB) expression in ccRCC cell lines was assessed by Western blot (WB) and quantitative PCR (qPCR) experiments, with immunohistochemistry applied to measure the levels of GSDMB and programmed cell death protein 1 (PD-1). **Results:** A prognostic risk model was developed using nine genes related to pyroptosis (*AIM2*, *CASP5*, *GSDMB*, *GSDMD*, *NLRP7*, *NOD2*, *PYCARD*, *SCAF11*, and *NLRP6*), employing both univariate Cox and LASSO regression analyses. Based on the median risk score, ccRCC samples were divided into high- and low-risk categories, with Kaplan-Meier analysis revealing poorer survival rates for the high-risk group. Time-dependent receiver operating characteristic curve analysis confirmed the predictive performance of the model for ccRCC prognosis. Furthermore, a nomogram with calibration plots was developed to predict 1-, 3-, and 5-year survival probabilities for patients with ccRCC. Notably, these pyroptosis-related genes were strongly correlated with immune cell infiltration, including cytotoxic cells, CD56bright natural killer cells, and T helper cells. Subsequently, qPCR and WB analyses confirmed elevated GSDMB expression in ccRCC cells, and immunohistochemistry demonstrated a strong correlation between GSDMB and PD-1 expression. **Conclusions:** Pyroptosis-associated genes, namely *AIM2*, *CASP5*, *GSDMB*, *GSDMD*, *NLRP7*, *NOD2*, *PYCARD*, *SCAF11*, and *NLRP6*, are promising prognostic biomarkers for ccRCC, and may serve as prognostic biomarkers for predicting patient survival and informing immunotherapy strategies.

Keywords: pyroptosis; prognostic model; LASSO Cox regression; gasdermin B; immune infiltration

1. Introduction

Originating in the epithelial lining of the renal tubules, Renal Cell Carcinoma (RCC) stands as the second most prevalent malignancy within the adult urinary tract, surpassed only by bladder cancer [1]. Among its various subtypes, clear cell renal cell carcinoma (ccRCC) predominates, representing 70–80% of all RCC cases. Characterized by an aggressive nature and poor prognosis [2,3], ccRCC is often identified at a late stage because it begins subtly and progresses quickly [4]. While targeted therapy has extended survival rates, overcoming drug resistance during prolonged treatment remains a significant challenge [5]. Immune therapy, especially immune checkpoint inhibitors, shows great promise as a treatment for patients with ccRCC [6]; however, ccRCC generally has a poor prognosis, and it is important to mitigate immune-related adverse effects [7,8,9,10]. There is a constant demand for the identification of new biomarkers for early detection and improved prognostic accuracy in ccRCC.

Pyroptosis represents a newly identified pattern of programmed cellular death that is distinct from apoptosis. The process is initiated by the gasdermin (GSDMB) family and involves the formation of pores in the cell membrane, leading to cell swelling and bursting, which releases their contents. The gasdermin family, which consists of six human homologs— GSDMA–D, GSDME (aka DFNA5), and pejvakin (PJVK, aka DFNB59)—is crucial in the process of pyroptosis. Distinct from apoptosis, this programmed

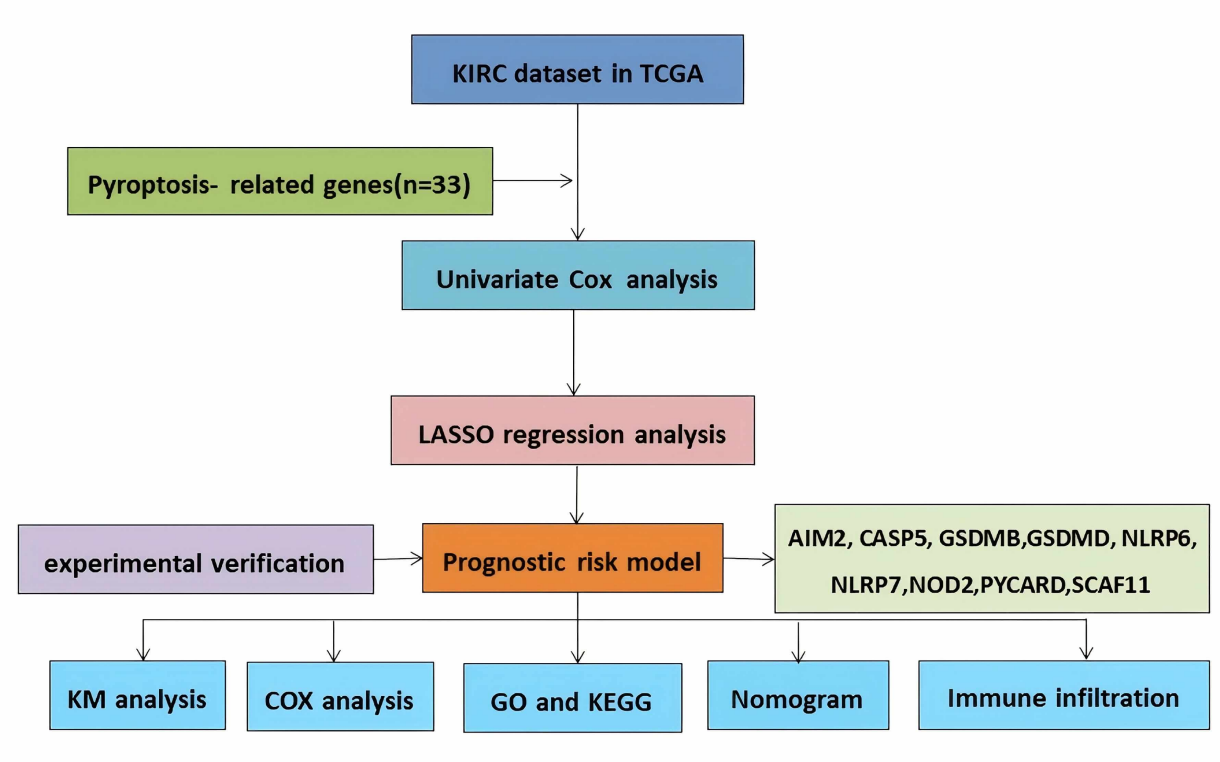

Fig. 1. Comprehensive workflow diagram for data analysis. Schematic overview of the study design, including sample screening, inclusion, and analytical stages. Patients with ccRCC from three independent cohorts—TCGA, Gene Expression Omnibus (GEO), and West China Hospital (WCH)—were assessed. Using the TCGA training cohort, a transcription factor-based prognostic signature was constructed via Cox and LASSO regression analyses. The model's prognostic and immunological significance was analyzed. External validation was performed in GEO (GSE40435 and GSE126964) and CPTAC cohorts, with further functional assays in ccRCC cell lines. Abbreviations: KIRC, Kidney Renal Clear Cell Carcinoma; TCGA, The Cancer Genome Atlas; LASSO, Least Absolute Shrinkage and Selection Operator; KM, Kaplan-Meier; GO, Gene Ontology; KEGG, Kyoto Encyclopedia of Genes and Genomes.

cell death is induced by the development of membrane pores, causing the cell to swell, rupture, and release cellular contents [11]. Pyroptosis is initiated through two distinct pathways. The classical pathway involves the activation of caspase-1 (CASP1), which cleaves GSDMD. Conversely, the nonclassical pathway is triggered by bacterial lipopolysaccharide binding to CASP4/5/11, which also results in GSDMD cleavage [12,13]. More studies are highlighting the significance of pyroptosis in the progression of cancer. GSDMB, a member of the GSDM family, is known for its pyroptosis-like activity and is overexpressed in various cancers, and likely contributing to progression and metastasis. Nonetheless, its precise prognostic significance and connection with immune infiltration in ccRCC have yet to be completely clarified.

Thus, comprehending how pyroptosis influences cancer growth and advancement, and establishing a corresponding prognostic model, is essential for improving ccRCC treatment. Furthermore, genes related to pyroptosis can serve as prognostic indicators in multiple forms of cancer, including lung [14], liver [15,16], and breast [17] cancers, by enabling the development of specialized risk models. To date, no pyroptosis-focused prognostic signature has been established for predicting outcomes in patients with ccRCC. Consequently, it is vital to develop a new model based on pyroptosis-associated genes to predict patient survival.

This study focused on creating a prognostic model using genes linked to pyroptosis to forecast the outcomes for patients with ccRCC. We confirmed that GSDMB is expressed in ccRCC tissues, providing a potential therapeutic target. Our study thoroughly examined the predictive significance of genes related to pyroptosis and their links to clinical characteristics, suggesting their promise as prognostic indicators and new therapeutic targets.

2. Materials and Methods

2.1 Data Collection and Processing

Pyroptosis-associated genes were found by exploring PubMed (https://pubmed.ncbi.nlm.nih.gov/) for 'pyroptosis' AND 'Homo sapiens' (PMID: 30842595, PMID: 31501419, PMID: 28813641, PMID: 25879280) following the workflow in Fig. 1, resulting in the selection of approximately 33 pyroptosis-related genes. Transcriptomic

profiles paired with clinical metadata for 541 ccRCC patients and 72 normal specimens were harvested from The Cancer Genome Atlas (TCGA) database (https://portal.gdc.cancer.gov/). The expression datasets GSE40435 and GSE126964, which included 101 ccRCC samples and 55 ccRCC samples separately, were sourced from the Gene Expression Omnibus (GEO) (https://www.ncbi.nlm.nih.gov/geo/). GSE245372 includes 15 non-metastatic ccRCC samples treated with neoadjuvant nivolumab to assess immunomodulatory response. Differential expression analysis of TCGA data was executed using the 'DESeq2' package with a false discovery rate (FDR) <0.05. The study found 20 genes with different expression levels in tumor samples compared to normal ones. A univariate Cox analysis was employed to determine prognostic pyroptosis-related genes (PRGs) associated with overall survival (OS) ($p < 0.05$). Finally, a model for prognosis was formulated using PRGs that showed both differential expression and prognostic significance within the TCGA cohort.

2.2 Enrichment Analysis of Differentially Expressed Pyroptosis-Related Genes

The delineation of differentially expressed PRGs (DEPRGs) distinguishing ccRCC from normal tissues was undertaken utilizing R software, applying thresholds of |log2 (fold change, FC)| >0.5 and FDR <0.05. The functional roles of these genes were analyzed using Gene Ontology (GO) and Kyoto Encyclopedia of Genes and Genomes (KEGG) analyses. The enrichment analysis of DEPRGs for biological processes (BP), cellular components (CC), and molecular functions (MF) was executed using the R package 'clusterprofiler'. The same methodological framework was applied to perform KEGG enrichment analysis, with statistical significance defined as a *p*-value less than 0.05.

2.3 Protein–Protein Interaction Analyses

Protein–protein interaction (PPI) data for DEPRGs were retrieved from The Search Tool for the Retrieval of Interacting Genes/Proteins (STRING) database and visualized using Cytoscape 3.9.0 (CA, USA, https://cytoscape.org) [18]. A high-confidence interaction score of >0.7 was applied to define significant interactions.

2.4 Development of a Prognostic Model Using PRGs

To prevent overfitting, a prognostic model was formulated using (least absolute shrinkage and selection operator, LASSO)-penalized Cox regression analysis on overlapping PRGs, which was subsequently refined to identify key genes. Patient risk scores were determined by applying the formula: $\sum(X_J * coef_J)$, where X_j is the Z-score normalized expression of each DEPRG and $coef_J$ is its corresponding coefficient. Patients were categorized into high-risk and low-risk groups according to the median risk score from the TCGA cohort.

2.5 Pyroptosis Prognosis Model Evaluation

Using the R package (Vienna, Austria, https://www.r-project.org), we generated Kaplan-Meier plots to compare survival and risk profiles between the two groups. Then we investigated the correlation between clinicopathological characteristics and risk scores utilizing the 'Survival' package to identify unique prognostic variables. Finally, we used the 'survivalROC' package to construct receiver operating characteristic (ROC) curves and calculated the area under the curve (AUC) to determine the accuracy of the model's predictions. As a probability measure ranging from 0.5 to 1, a higher AUC indicates superior predictive accuracy, signifying, in this study, greater alignment between the actual and predicted OS.

2.6 Clinicopathological Data Combined With Pyroptosis Risk Score Signature

Prognostic predictors related to ccRCC were identified, including clinical features and the established Pyroptosis Risk Score. Univariate Cox regression analyzed the link between OS and the Pyroptosis Risk Score, whereas multivariate analysis determined its value as an independent prognostic factor. Using the 'rms' package, a nomogram was developed to comprehensively evaluate patient survival by integrating the Pyroptosis Risk Score with clinicopathological variables (age, sex, histologic grade, and pathologic stage). Similarly, decision curve analyses (DCAs) were performed over 1-, 3-, and 5-year spans to assess the clinical utility of existing synthetic nomograms, with the x-axis depicting the threshold probability percentage and the y-axis representing net benefit.

2.7 Analysis of Immune Cell Infiltration

The marker genes were obtained for each of the 24 different immune cell types, according to a study by Bindea et al. [19]. Using the single-sample gene set enrichment analysis (GSEA) method, the infiltration of 24 different types of immune cells into the tumor was examined. The Xiantao tool was used to analyze PRG expression, perform GSEA, and explore ccRCC–immune system interactions, whereas TISIDB was used to confirm the relationship between GSDMB and immune components, including cells, immunostimulators, and inhibitors [20].

2.8 Immunohistochemistry

A total of 13 patients surgically diagnosed with ccRCC via pathological staining at our hospital were involved in this investigation. The use of tissue samples was permitted by all patients through written informed consent, and the research protocol was approved by our institutional review board (Approval No. 2025-MNWK-K-002). The preserved paraffin blocks were retrieved and re-sectioned. The slides were baked at 65 °C for more than 2 hours to ensure tissue dryness. Then, the standard immunohistochemistry procedure was followed. Briefly, after xylene

deparaffinization, the slides were rehydrated using a gradient ethanol series. The slides underwent an antigen retrieval system in EDTA buffer (pH 8.0) at 95 °C under high pressure for 15 minutes, followed by a gradual cooling period. Once the slides were removed, the tissue was circled using an immunohistochemistry pen. To quench endogenous peroxidase activity, sections were exposed to 3% hydrogen peroxide and subsequently incubated with 5% bovine serum albumin for 40 minutes to mitigate nonspecific binding. Following this, the tissue specimens were subjected to an overnight incubation at 4 °C in the presence of the specified primary antibodies: GSDMB (1:400, 12885-1-AP; Proteintech Group, Rosemont, IL, USA) and programmed cell death protein 1 (PD-1) (1:500, 18106-1-AP; Proteintech). After removing the primary antibody, following a 30-minute room temperature incubation with a secondary antibody, the samples were stained using DAB, hematoxylin counterstaining, dehydration, and mounting. The Digital Slide Imaging System (DS-120/DS-600/PA-1100) was used to perform digital slide scanning, with subsequent analyses conducted using ImageJ software (National Institutes of Health, Bethesda, MD, USA). Staining intensity was quantified using the H-Score formula: $\sum(pi \times i)$ = (% of weak intensity × 1) + (% of moderate intensity × 2) + (% of strong intensity × 3).

2.9 Cell Culture

To functionally validate the prognostic gene identified from TCGA, we performed *in vitro* cell culture experiments. These experiments were aimed at determining the expression pattern of the target gene in ccRCC cell lines and evaluating its effects on tumor cell proliferation, migration, and invasion. HK-2, Caki-1,786-O, and A498 cell lines were obtained from the American Type Culture Collection located in Manassas, VA, USA. HK-2 cells were maintained in DMEM/F-12 medium provided by Gibco, Waltham, MA, USA. A498 cells were cultured in MEM (Procell, Wuhan, China). Caki-1 and 786-O cells were cultured in RPMI 1640 medium (Gibco). All media included a supplement of 10% fetal bovine serum from HyCyte, Suzhou, China, and 1% penicillin/streptomycin from Invitrogen, Waltham, MA, USA. Cells were incubated at 37 °C in a 5% CO_2 incubator. All cell lines were validated by STR profiling. All cell lines were regularly checked for mycoplasma contamination with a commercial detection kit from Vazyme Biotech Co., Ltd., Nanjing, China, and were confirmed to be free of mycoplasma.

2.10 Quantitative PCR

The EZ-press RNA Purification Kit (EZBioscience, Houston, TX, USA) was used to extract total RNA from these cells, following the instructions provided by the manufacturer. IMPLEN GmbH's Nanophotometer N50, located in Munich, Germany, was employed to determine the RNA concentration and purity. Subsequently, reverse transcription was conducted with the Hifair® III 1st Strand cDNA Synthesis SuperMix (Yeasen Biotechnology, Shanghai, China). The quantitative PCR (qPCR) reaction system was prepared using ChamQ SYBR qPCR Master Mix (Vazyme), cDNA, primers, and DEPC-treated water, and was performed in a fluorescence qPCR detection system (BIOR Technology, Hangzhou, China). Data were normalized against GAPDH, with relative quantification determined using the $2^{-\Delta\Delta ct}$ formula. The primer sequences (obtained from Sangon, Shanghai, China) were:

GSDMB: Forward primer (ATGTAGACTCAACGGGAGAGTT), Reverse primer (GTAGCCAGATACTGCTGGGATA);

GAPDH: Forward primer (CTCCTCAGTGCATGTA), Reverse primer (GTTGAGCACAGGGTACTTTATTG).

2.11 Western Blot

Cell samples were lysed on ice for at least 10 minutes with RIPA buffer (Beyotime, Shanghai, China) comprising PMSF and a protease inhibitor, with intermittent shaking. Following centrifugation at 12,000 ×g for 15 minutes at 4 °C, the resultant supernatant was extracted. Proteins were quantified using the BCA Protein Assay Kit (GlpBIO Technology, Montclair, CA, USA), followed by normalization. The samples were separated using 10% SDS-PAGE and then transferred onto a 0.45 µm PVDF membrane. Proteins were initially blocked at room temperature using a quick blocking buffer from Epigentek, Farmingdale, NY, USA, and then incubated overnight at 4 °C with primary antibodies targeting GSDMB (1:1000, 12885-1-AP; Proteintech) and GAPDH (1:50,000, 60004-1-Ig; Proteintech). Subsequently, the membrane was rinsed with 1× TBST and then incubated with a secondary antibody for 1.5 hours at room temperature. Signals were detected using the Ultra High Sensitivity ECL Kit (GlpBIO, Shanghai, China) and imaged on the Vilber Imaging System (Collégien, Marne-la-Vallée, France), with GAPDH serving as the internal reference.

2.12 Statistical Analyses

Results are displayed as the mean ± standard deviation. Statistical analyses between pairs of groups were conducted utilizing *t*-tests, while comparisons across multiple groups were performed via one-way analysis of variance. A *p*-value of less than 0.05 was used to determine statistical significance. Pearson's correlation was employed to examine the relationships between continuous variables. Univariate and multivariate Cox proportional hazards regression analyses were performed to evaluate the association between gene expression levels and patient survival. The calculation of hazard ratios (HRs) included 95% confidence intervals (CIs). Variables with a *p*-value under 0.05 from the univariate analysis were incorporated into the multivariate Cox model.

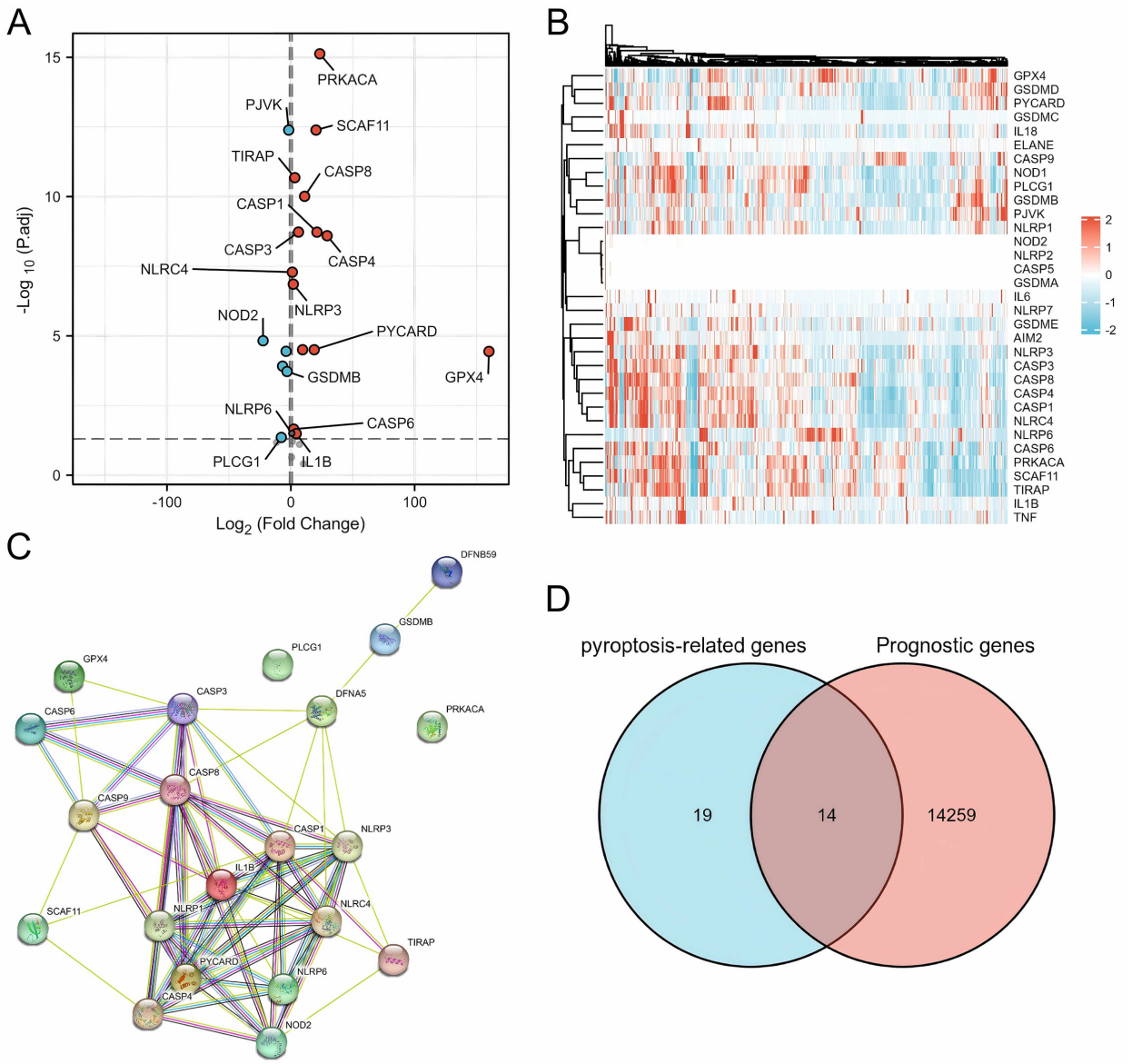

Fig. 2. DEPRGs between ccRCC and normal tissues. (A) Volcano plot shows PRGs, where upregulated genes appear as red dots and downregulated genes appear as blue dots. (B) Heatmap displays the differential expression pattern of PRGs, with red representing upregulation and blue representing downregulation. (C) PPI network displays interactions between genes linked to pyroptosis. (D) Venn diagram showing the 14 overlapping genes (*AIM2*, *CASP5*, *ELANE*, *GSDMB*, *GSDMD*, *GSDME*, *IL6*, *NLRP6*, *NLRP7*, *NOD2*, *PJVK*, *PYCARD*, *SCAF11*, and *TIRAP*).

3. Results

3.1 Identification of DEPRGs in ccRCC

The study's workflow is illustrated in Fig. 1. The training set consisted of gene expression, prognosis, and survival data from 541 patients with ccRCC and 72 normal samples. Based on DESeq2 analysis, 20 of 33 investigated PRGs were differentially expressed, defined by a |log2 (fold change)| >1.2 and FDR <0.05. Analysis of patients with ccRCC revealed 14 upregulated and 6 downregulated genes, as shown by volcano plots and heatmaps. (Fig. 2A,B,D). The PPI interaction network for these DEPRGs is shown in Fig. 2C.

3.2 Development of a Predictive Model Utilizing PRGs

Univariate Cox regression analysis (Fig. 3A) identified nine significant PRGs ($p < 0.05$): seven risk genes (absent in melanoma 2 [*AIM2*], *CASP5*, *GSDMB*, *GSDMD*, NLR family pyrin domain containing 7 [*NLRP7*], nucleotide-binding oligomerization domain-containing protein 2 [*NOD2*], and apoptosis-associated speck-like protein containing a CARD [*PYCARD*]) and two protective genes (SR-related CTD-associated factor 11 [*SCAF11*] and *NLRP6*). Three genes related to pyroptosis were identified as significant prognostic markers through multivariate Cox regression analysis: one risk fac-

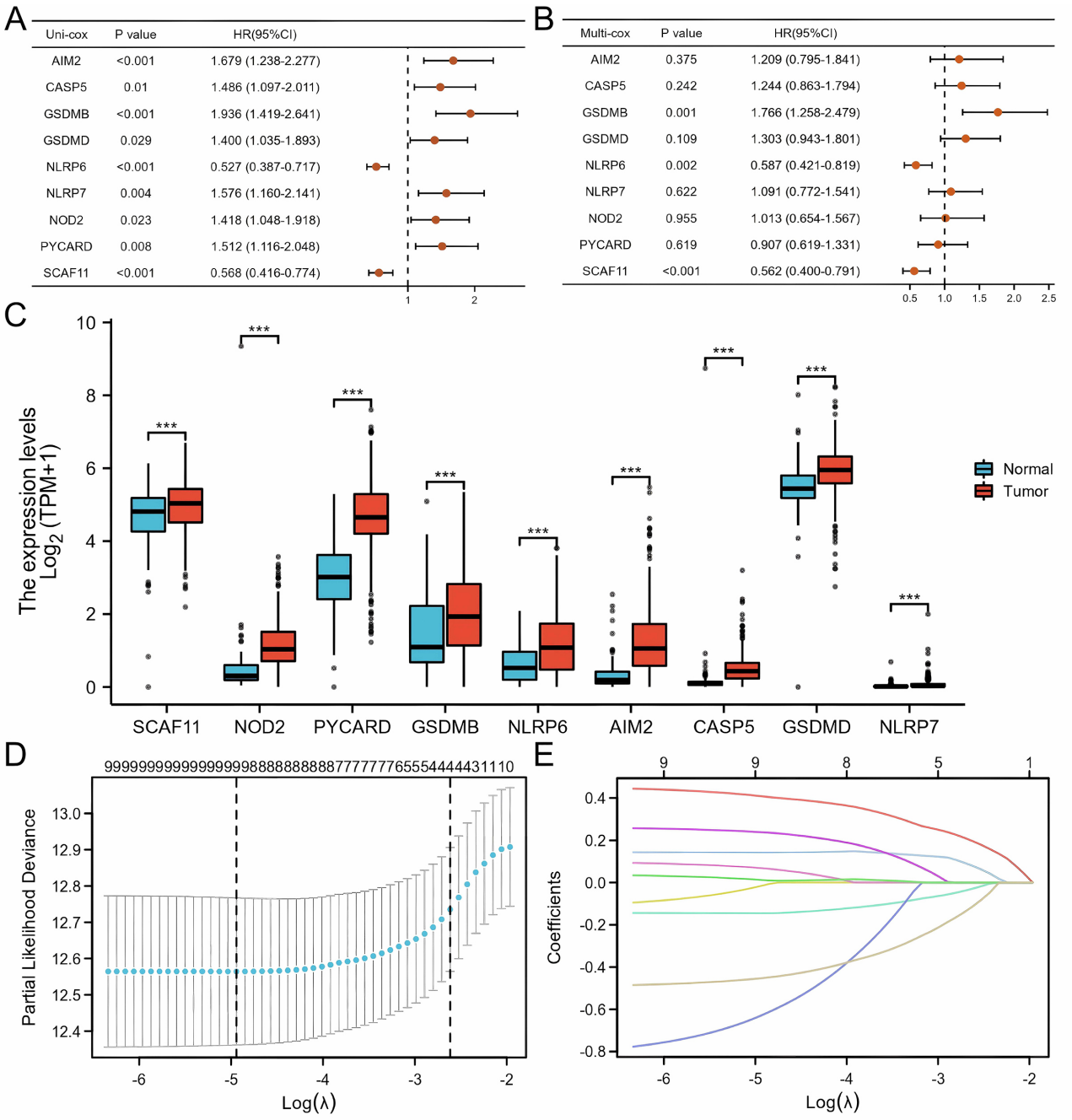

Fig. 3. Creation of a risk assessment model utilizing genes linked to pyroptosis within the TCGA cohort. (A) Differentially expressed genes associated with pyroptosis were analyzed using univariate Cox regression, with statistical significance established at $p < 0.05$. (B) Genes identified from univariate Cox regression analysis were further examined utilizing multivariate Cox regression. (C) Box plots depicting expression variations of PRGs, where red boxes represent tumor samples and blue boxes indicate control specimens. (D) Parameter optimization through cross-validation within the LASSO regression model. (E) LASSO coefficient profiles. *** $p < 0.001$.

tor and two protective factors (Fig. 3B). Boxplots revealed the significant upregulation of all nine genes associated with pyroptosis (Fig. 3C). After performing univariate Cox regression, LASSO regression was utilized to create a prognostic model (Fig. 3D,E) using the specified PRGs: *AIM2*, *CASP5*, *GSDMB*, *GSDMD*, *NLRP7*, *NOD2*, *PYCARD*, *SCAF11*, and *NLRP6*. The following formula was used to calculate the prognostic index for each cancer sample: Risk score = Level of AIM2 expression × 0.142480436 + Level of CASP5 expression × 0.238226528 + Level of GSDMB expression × 0.408821333 + Level of GSDMD expression × (–0.016482042) + Level of NLRP6 expression × (–0.145096111) + Level of NLRP7 expression × (–0.630286614) + Level of NOD2 expression × 0.068539303 + Level of PYCARD expression × 0.012641442 + Level of SCAF11 expression × (–0.453262898). To assess how well

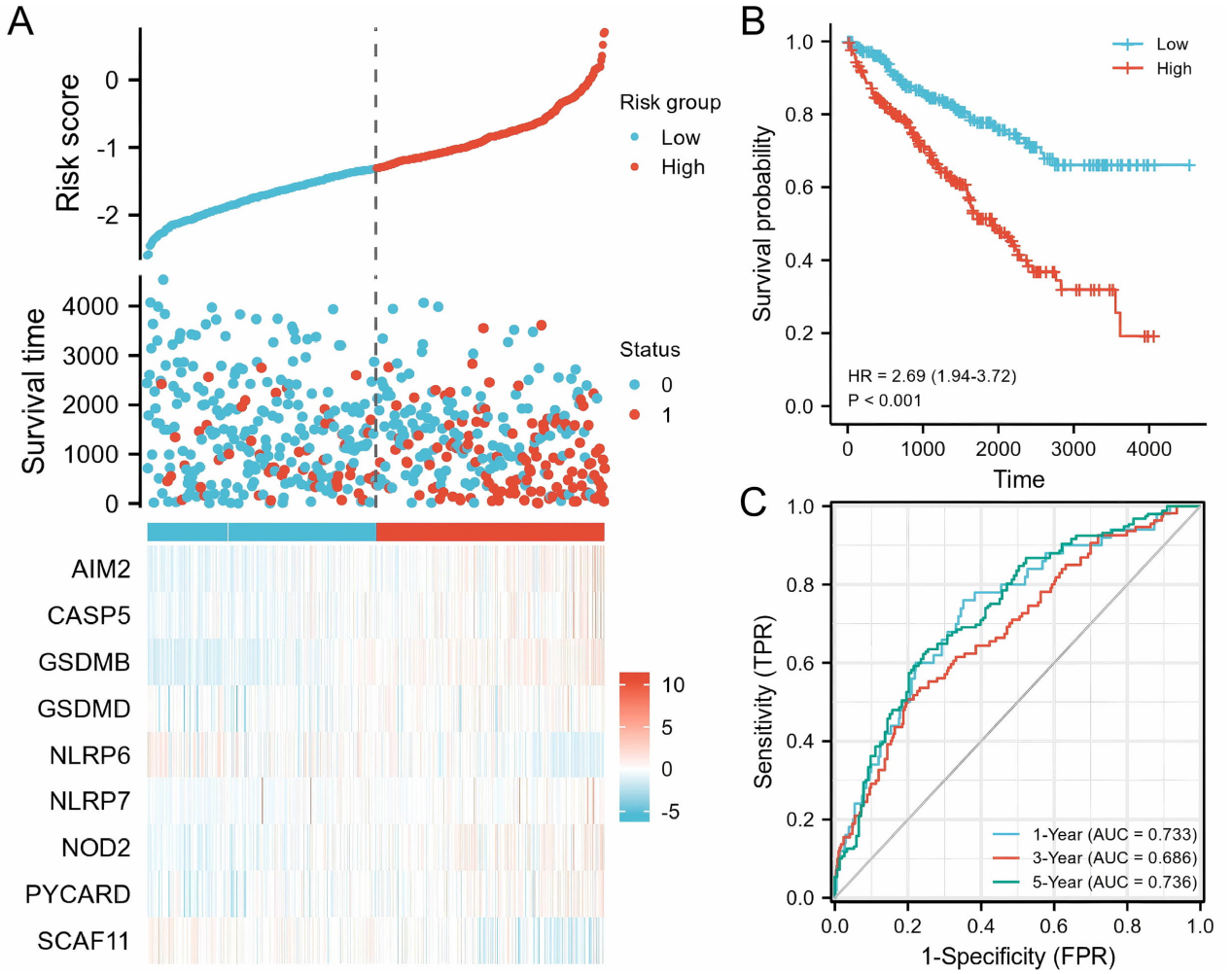

Fig. 4. Verification of the risk model in the TCGA dataset. (A) Patients were stratified into two groups based on the median risk score value. The survival status of patients with ccRCC in high- and low-risk groups is illustrated, with blue indicating survival and red signifying death. The expression pattern of nine PRGs is presented through heat map visualization. The low-risk group is represented in blue, and the high-risk subset is indicated in red. (B) OS depicted by Kaplan-Meier curves for patients categorized as high risk and low risk. (C) ROC curve was applied to examine the predictive capability of the risk score.

the pyroptosis-related model predicts outcomes in ccRCC patients, participants were categorized into high-risk and low-risk groups according to the median risk score. The high-risk group exhibited a higher mortality rate (Fig. 4A), and a less favorable prognosis, as evidence by Kaplan-Meier curves (HR = 2.69, 95% CI = 1.94–3.72; log rank $p <$ 0.001) (Fig. 4B). Time-dependent ROC assessment showed that the model's predictive accuracy for OS reached 0.733, 0.686, and 0.736 at 1, 3, and 5 years, respectively (Fig. 4C). The model's robustness was confirmed through validation in external cohorts (such as GSE40435, GSE126964, and CPTAC), wherein *GSDMB*, *GSDMD*, *PYCARD*, and *SCAF11* also exhibited marked overexpression in ccRCC, underscoring the predictive framework's considerable stability (**Supplementary Fig. 1**). These findings confirm that the PRG signature in the prognostic model accurately predicts ccRCC outcomes within the training cohort.

3.3 Clinical Utility of a Prognostic Risk Score Signature

We conducted both univariate and multivariate Cox regression analyses to examine the prognostic value of the established risk score signature. Univariate Cox regression analysis indicated that age, risk score, histologic grade, and pathologic stage, but not sex, were prognostic predictors in TCGA-Kidney Renal Clear Cell Carcinoma (Fig. 5A). Specifically, multivariate Cox regression analysis revealed that the risk score is an independent predictor (HR = 1.660, 95% CI = 1.295–2.128; log-rank $p < 0.001$) (Fig. 5B). DCA demonstrated that integrating the risk score signature with established clinical parameters yields enhanced clinical utility (Fig. 5C). These findings establish our risk score signature as a reliable, innovative biomarker for predicting prognosis.

Nomograms provide event probability predictions tailored to individual patient profiles by simplifying com-

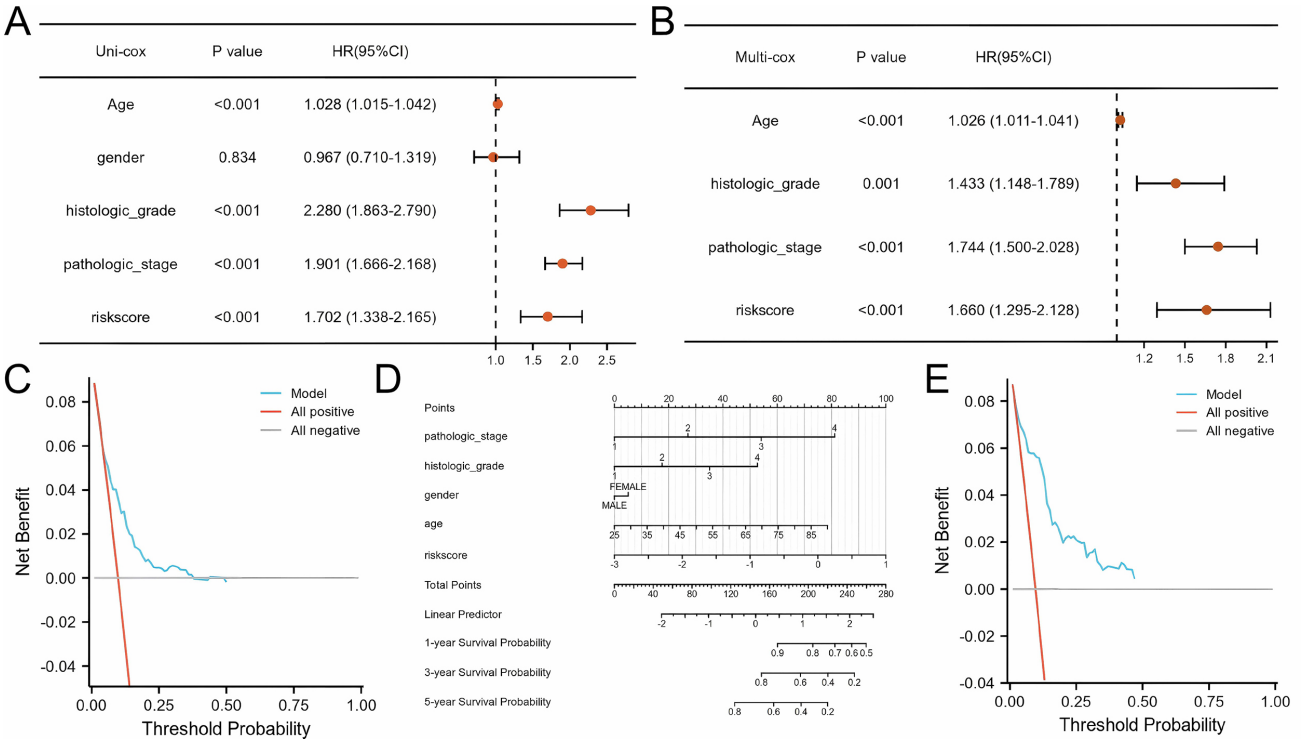

Fig. 5. Nomogram for predicting the survival probability of patients with ccRCC. (A) According to univariate Cox regression analysis, age, histological grade, pathological stage, and risk score were related to OS in patients with ccRCC. (B) The risk score was independently linked to OS in patients with ccRCC, as demonstrated by multivariate Cox regression analysis. (C) DCA to assess the net benefit of the risk score. The y-axis shows net benefit; the x-axis shows threshold probability. The 'All negative' line (grey horizontal line) represents the strategy of treating no patients (net benefit = 0). The 'All positive' line (red dashed line) represents the strategy of treating all patients. The model curve (blue line) represents the net benefit of using the risk score to guide clinical decisions. (D) To predict 1-, 3-, and 5-year OS in ccRCC, the nomogram incorporates five factors: age, histological grade, sex, pathological stage, and risk score. (E). DCA to evaluate the net benefit of the nomogram. The y-axis shows net benefit; the x-axis shows threshold probability. The 'All negative' line (grey horizontal line) represents the strategy of treating no patients (net benefit = 0). The 'All positive' line (red dashed line) represents the strategy of treating all patients. The model curve (blue line) represents the net benefit of using the nomogram to guide clinical decisions.

plex statistical prediction models into single numerical estimates. They are extensively used for tumor prognosis. As many clinical features have prognostic value in practice, we developed a nomogram that incorporates multiple clinicopathological features as well as a risk score signature to accurately assess patient prognosis. Fig. 5D illustrates how individual variable scores can be calculated, and provides a thorough assessment regarding the prediction of outcomes of patients with ccRCC. The DCA curve (Fig. 5E) also confirmed that the nomogram provides improved clinical utility when combined with multiple clinical characteristics.

3.4 Functional Enrichment Analysis

GO and KEGG analyses of the 20 DEPRGs in ccRCC revealed their potential signaling pathways. Based on BP analysis, DEPRGs demonstrated substantial enrichment in cysteine-type endopeptidase activity activation, which functions in apoptotic processes and interleukin-1 beta (IL-1β) generation. CC analysis identified the inflammasome complex as the most markedly altered pathway. Within MF, significant enrichment manifested in cysteine-type endopeptidase activity contributing to apoptotic processes, cysteine-type peptidase activity, and cysteine-type endopeptidase activity (Fig. 6A). The 10 most markedly enriched signaling pathways identified through KEGG analysis are as follows: the NOD-like receptor signaling pathway, Salmonella infection, legionellosis, pertussis, influenza A, Yersinia infection, shigellosis, cytosolic DNA-sensing pathway, tuberculosis, and pathogenic *Escherichia coli* infection (Fig. 6B). These findings indicate that PRGs participate in BP beyond pyroptosis.

3.5 Prognostic Analysis of Nine PRGs in ccRCC

To investigate the importance of risk genes associated with pyroptosis in different types of cancer, we examined the relationship between TCGA patient OS and expression of these model genes. We constructed an OS heatmap for these genes (Fig. 7A) and performed Kaplan-Meier anal-

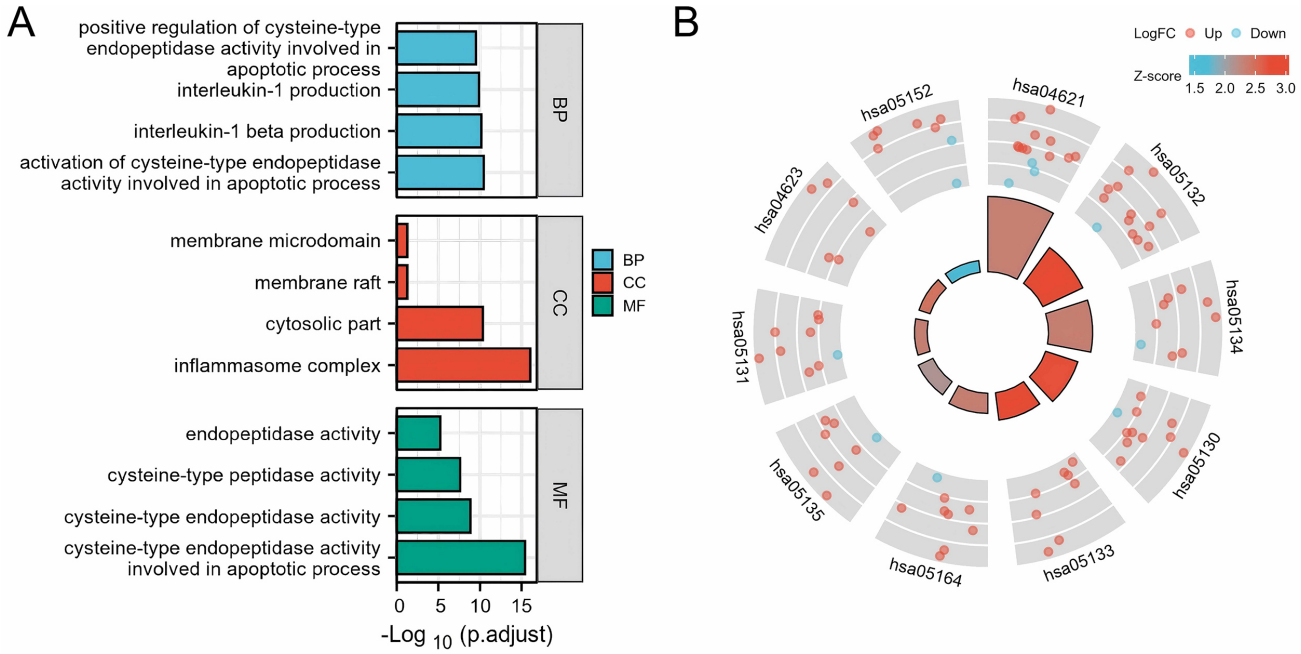

Fig. 6. GO and KEGG enrichment analyses. (A) GO analysis was conducted on 20 genes with differential expression linked to pyroptosis. The bar chart shows the top enriched GO terms in the BP, CC, and MF categories. (B) Top 10 KEGG pathways enriched in the analysis of 20 differentially expressed genes linked to pyroptosis. Each column in the inner circle corresponds to an item. The higher the column, the higher the reliability of the corresponding ID and the smaller the *p*-value. The outer ring represents the molecules included in the entry, where molecules with a positive logFC are labeled as Up, and those with a negative logFC are labeled as Down.

ysis to evaluate the association with clinical outcomes in patients with ccRCC. As shown in Fig. 7B–E, and Fig. 7G–I, the higher expression of *AIM2*, *CASP5*, *GSDMB*, *GSDMD*, *NLRP7*, *NOD2*, *PYCARD*, and lower expression of *SCAF11*, *NLRP6* (Fig. 7J and Fig. 7F) were correlated with a worse prognosis in patients with ccRCC.

3.6 Relationship Between GSDMB and Immune Molecules

The link between *GSDMB* levels and tumor-infiltrating immune cells in ccRCC was analyzed using the Xiantao tool (Shanghai, China, https://www.xiantao.love/). The outcomes indicated a significant positive link between *GSDMB* expression and various tumor-infiltrating lymphocytes (TILs), specifically cytotoxic cells, CD56bright natural killer cells (CD56bright), and T helper cells (Fig. 8A). There were also significant negative correlations observed between *GSDMB* expression levels and other TILs, such as T gamma delta cells and mast cells. Similar results were obtained upon analysis of the 28 immune-associated TIL types in the TISIDB database (Fig. 8B). Using the TISIDB database, we further investigated the relationships between *GSDMB* expression and various immune indicators, including both immune inhibitors and stimulators. Fig. 8C shows the high positive correlation between *GSDMB* expression levels and immunostimulatory factors such as tumor necrosis factor receptor superfamily member 18 (TNFRSF18; r = 0.487), TNFRSF14 (r = 0.496), cluster of differentiation (r = 0.311), and TNFRSF25 (r = 0.795). These results suggest that the infiltration of TILs and immune molecules may be pivotal in determining the outcomes of patients with ccRCC. Considering the significance of immune checkpoint inhibition therapy for individuals with ccRCC, the association between GSDMB expression and different immune checkpoint markers was investigated. As illustrated in Fig. 8D, *GSDMB* expression exhibited a significant positive correlation with lymphocyte activation gene 3 (LAG-3, r = 0.411), PD-1 (r = 0.375), and cytotoxic T-lymphocyte-associated antigen 4 (CTLA-4; r = 0.479). Collectively, these results imply that the gene signature associated with pyroptosis could affect how patients with ccRCC respond to immunotherapy.

3.7 GSDMB Expression is Linked to T-cell Exhaustion Infiltration Level in ccRCC

Using the TISIDB database, we investigated the link between GSDMB and T-cell exhaustion in ccRCC, finding a positive correlation between GSDMB expression and PD-1. Consequently, immunohistochemical analysis confirmed this positive correlation (Fig. 9A). The expression of GSDMB and PD-1 was markedly elevated in ccRCC tissue relative to normal controls. GSDMB and PD-1 were more highly expressed in ccRCC tissues compared to paired normal kidney samples ($p < 0.01$; Fig. 9B,C), with a strong positive correlation between GSDMB and PD-1 levels (Fig. 9D). Moreover, upregulated GSDMB correlated with increased T-cell exhaustion infiltration. These findings, in-

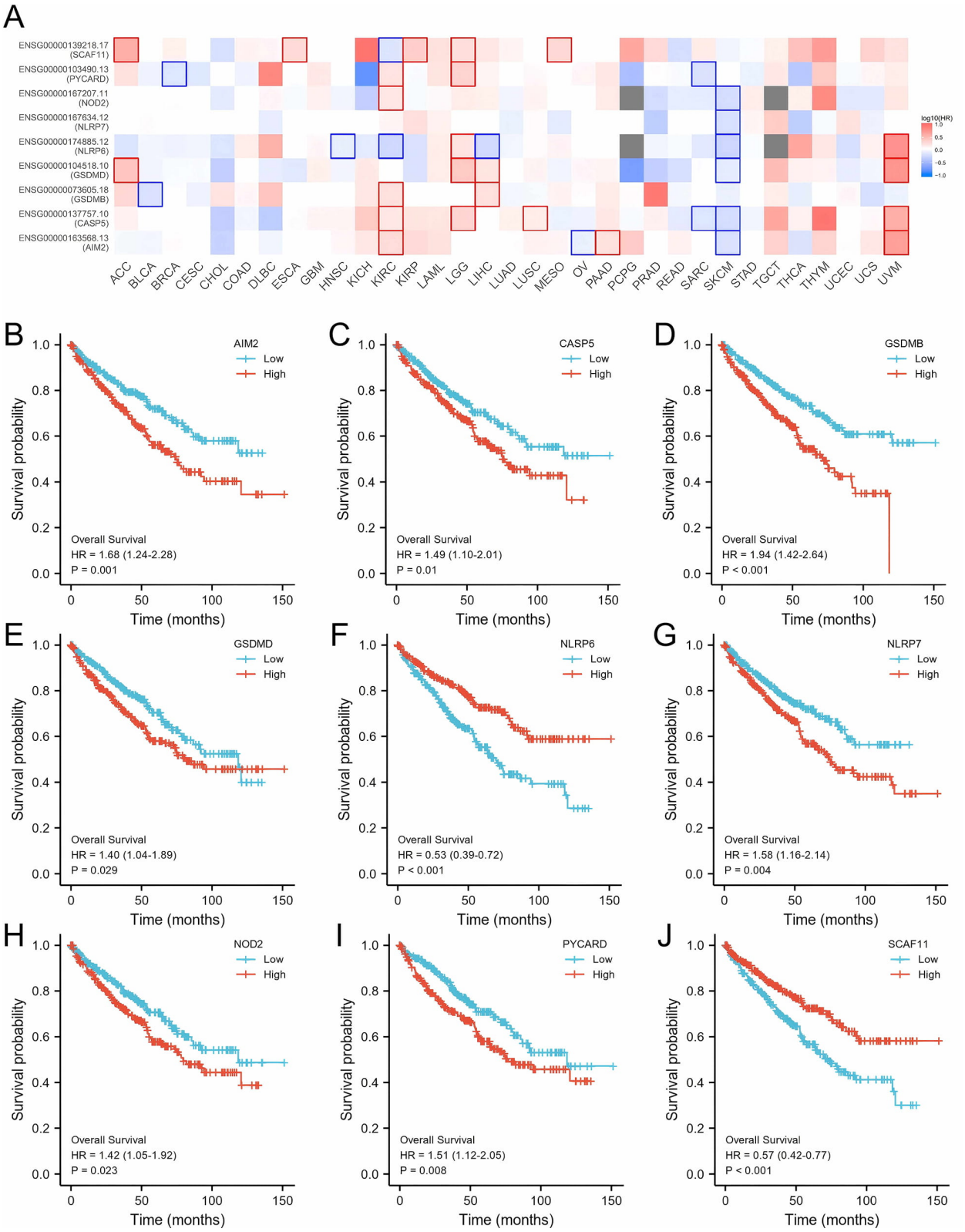

Fig. 7. Prognostic analysis of nine PRGs in ccRCC. (A) Construction of a heatmap for the genes associated with OS. Red boxes represent the high expression of genes in this tumor type, associated with shorter OS, while blue boxes represent the low expression of genes in this tumor type, associated with shorter OS. (B–J) Survival analysis was conducted to explore the relationship between the expression of *AIM2*, *CASP5*, *GSDMB*, *GSDMD*, *NLRP6*, *NLRP7*, *NOD2*, *PYCARD*, *SCAF11*, and ccRCC.

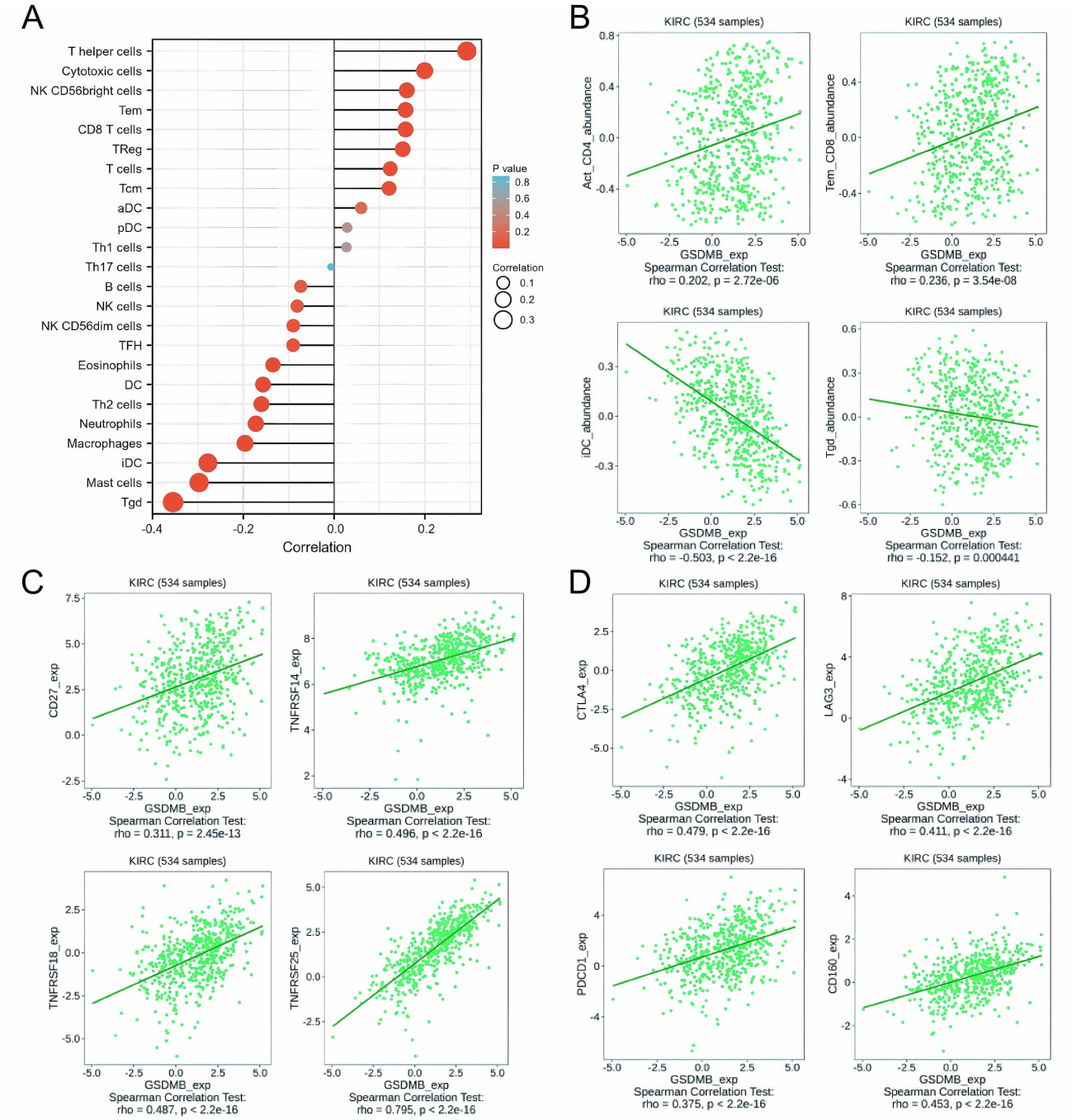

Fig. 8. Analysis of the link between immune infiltration and *GSDMB* level. (A) Link between *GSDMB* level and immune cell populations. The color of the circle corresponds to the *p*-value, and the size of the circle corresponds to the absolute value of the correlation coefficient. The higher the degree of correlation, the larger the circle. (B) Relationship between *GSDMB* levels and partial lymphocyte immune infiltration was validated through the TISIDB database. (C) Associations of *GSDMB* expression with immunostimulators (cluster of differentiation 27 [CD27], TNFRSF14, TNFRSF18, and TNFRSF25). (D) Associations of *GSDMB* expression with immunoinhibitors (CTLA4, LAG3, PD-1, and CD160).

dicating higher *GSDMB* mRNA levels in ccRCC, were validated by WB and qPCR (Fig. 9E). WB analysis also demonstrated that ccRCC cells exhibit increased basal levels of GSDMB protein (Fig. 9F).

4. Discussion

Recent research highlights the significant impact of pyroptosis—a form of programmed cell death mediated by CASP1 or CASP11—on cancer development [21,22]. PRGs play distinct roles across different cancer types. While cellular destruction releases inflammatory mediators

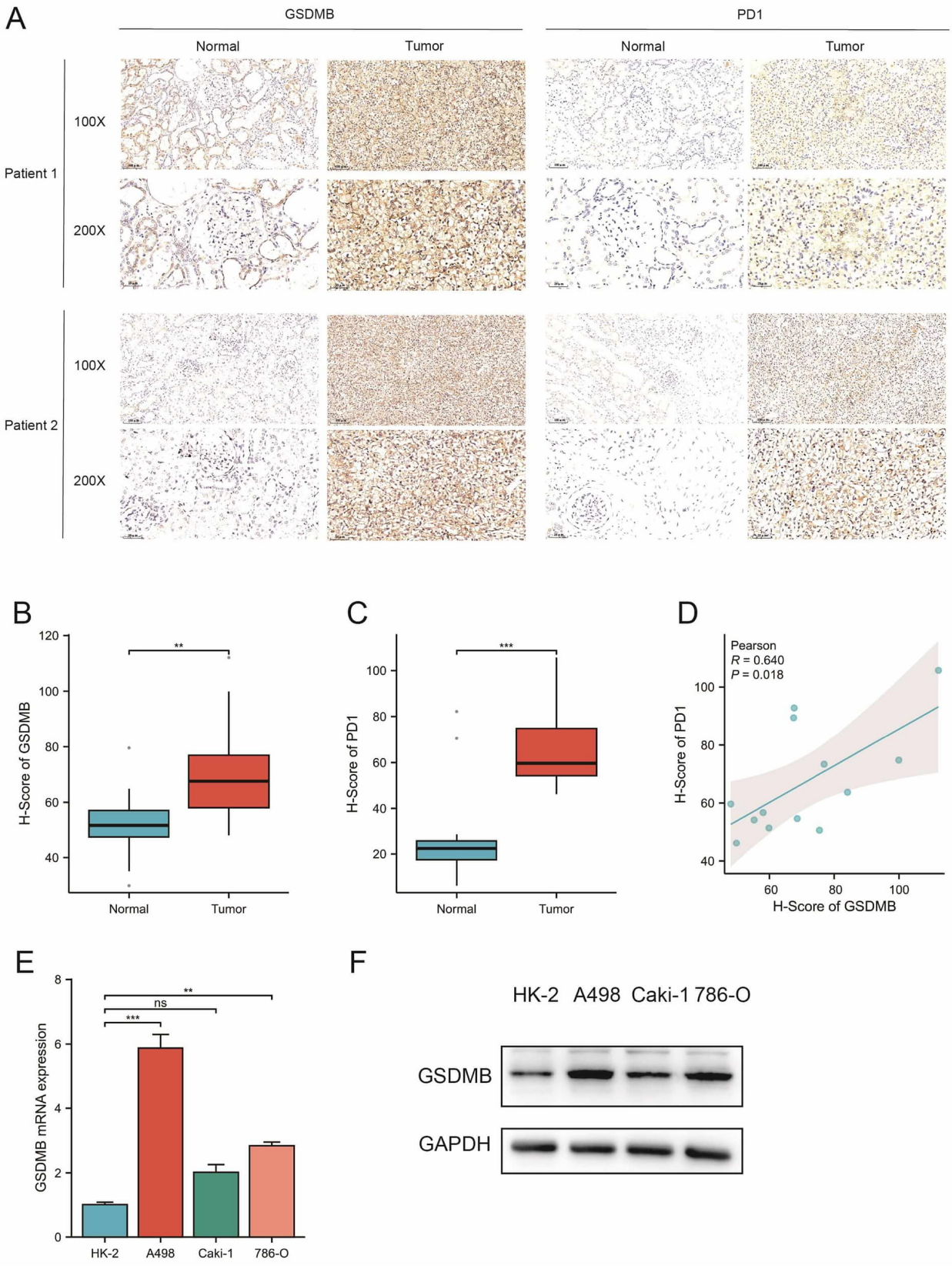

Fig. 9. Validation of the expression of GSDMB and the relationship between GSDMB and PD-1 levels in ccRCC tissues. (A) Immunohistochemistry (IHC) of ccRCC and normal tissues. Scale bar = 25 μm (200×) or 100 μm (100×). (B) IHC scores of GSDMB in ccRCC and normal tissues. (C) IHC scores of PD-1 across ccRCC and normal tissues. (D) Relationship between GSDMB and PD-1 levels as determined by IHC scores. (E) qPCR analysis of *GSDMB* in ccRCC cell lines (A498, Caki-1, and 786-O) and HK2 cells. (F) WB analysis of GSDMB in ccRCC cell lines (A498, Caki-1, and 786-O) and HK2 cells. ns, not significant; ** $p < 0.01$; *** $p < 0.001$.

that foster tumor growth, pyroptosis actively destroys tumor cells, making it a valuable target for cancer prognosis and treatment [23,24].

Despite the recent identification of many novel biomarkers for ccRCC prognosis, this study represents the first prognostic model specifically focused on pyroptosis. We identified 20 DEPRGs between normal renal tissues and tumor tissues. A novel risk prediction model was developed using LASSO Cox regression analysis, comprising nine PRGs: *AIM2*, *CASP5*, *GSDMB*, *GSDMD*, *NLRP7*, *NOD2*, *PYCARD*, *SCAF11*, and *NLRP6*. Several of these genes are known to be involved in ccRCC or other cancers, with GSDMB previously known as gasdermin-like protein. This suggests that *GSDMB* could play an important role in the metastasis and migration of cancer cells [25,26,27,28]. A number of articles have recently been published on the role of *GSDMB* in the oncogenesis of numerous cancer types, such as gastric cancer, cervical squamous cell carcinoma, and breast cancer [29,30,31].

Participants in the TCGA dataset were categorized into high-risk and low-risk groups according to the median risk value. Kaplan-Meier analysis indicated that patients in the high-risk group had reduced survival rates. The signature's predictive accuracy was evaluated using ROC analysis. Multivariate Cox regression, illustrated in a forest plot, confirmed the risk score as an independent prognostic factor for the TCGA population. GO and KEGG pathway analyses linked PRGs to IL-1β production, NOD-like receptor signaling, and IL-1 synthesis, emphasizing the essential function of the immune microenvironment in ccRCC progression. The established nomogram accurately predicted the OS of patients with ccRCC, with calibration plots confirming the strong predictive alignment.

GSDMB expression showed a positive correlation with multiple immune checkpoints, including CTLA-4, LAG-3, and PD-1. Immune checkpoint inhibitors, focusing mainly on PD-1, CTLA-4, and programmed death-ligand 1 (PD-L1), represent a significant advancement in cancer immunotherapy [32]. CTLA-4, which is found on the surface of T cells such as CD4+ helper and CD8+ cytotoxic types, functions as an immune checkpoint to manage T-cell activation and maintain immune homeostasis. Importantly, the enhanced CD8+ responses observed with anti-CTLA-4 therapy likely stem indirectly from CD4+ cell activation, given that CTLA-4 is chiefly present on CD4+ helper cells [33]. Tumors such as non-small cell lung cancer, RCC, melanoma, head and neck cancer, bladder urothelial cancer, and Hodgkin's lymphoma can be treated using PD-1/PD-L1 inhibitors, including nivolumab and pembrolizumab [34]. Recent research indicates that IBI315, a bispecific antibody targeting human PD-1 and HER2 (IgG1), combats malignancies by inducing *GSDMB*-mediated pyroptosis within cancer cells [35]. Analysis of GSE245372 revealed marked alterations in *GSDMB* expression preceding and following neoadjuvant Nivolumab therapy in ccRCC (**Supplementary Fig. 2**). Together, these findings identify *GSDMB* as a pro-oncogenic factor in ccRCC that regulates pyroptosis-related pathways, making it a promising therapeutic strategy.

VHL mutation or inactivation is one of the core molecular events in ccRCC and may affect tumor metabolism, angiogenesis, the immune microenvironment, and inflammatory responses through HIF-related pathways. By analyzing the TCGA gene mutation data, we found no difference in *GSDMB* expression between VHL wild-type and VHL mutant ccRCC samples (**Supplementary Fig. 3A**); regarding whether VHL status affects *GSDMB* and patient prognosis, our analysis showed that under VHL status, *GSDMB* expression still has predictive value for ccRCC prognosis ($p < 0.01$) (**Supplementary Fig. 3B**); additionally, under VHL status, the correlation between *GSDMB* and PD-1 expression remains strong (**Supplementary Fig. 3C**).

Although pyroptosis is a form of programmed cell death that should theoretically eliminate tumor cells, our finding that its elevated expression predicts a poorer prognosis in ccRCC is not as contradictory as it seems. Several non-mutually exclusive mechanisms can explain this paradox. First, the high expression of PRGs might indicate chronic inflammation rather than effective tumor cell pyroptosis [36]. Persistent inflammasome activation leads to the sustained release of IL-1b [37] and IL-18 [38], which can promote tumor proliferation, angiogenesis, and metastasis. Second, these genes show high expression levels in tumor cells as well as in infiltrating immune cells, such as: tumor-associated macrophages and neutrophils [39]. Thus, their expression may indicate inflammatory tumor microenvironment remodeling rather than direct tumor cell death. Third, chronic pyroptotic signaling can contribute to immune exhaustion by increasing the expression of immune checkpoint molecules such as PD-L1, thereby impairing antitumor immunity [40].

Despite revealing the role of *GSDMB* in ccRCC, our study still had limitations. First, the limited public database of clinical data restricted our ability to conduct more in-depth subgroup analyses. Second, the PRG signature was developed and validated using retrospective cohorts from public databases, lacking validation with real-world clinical data. Finally, our investigation into *GSDMB* expression in ccRCC tissues was only preliminary. Future studies, including well-designed animal studies, are needed to fully clarify *GSDMB*'s specific role, underlying mechanisms, and impact on the immunotherapy response.

5. Conclusions

In this research, we created a predictive model utilizing nine genes—*AIM2*, *CASP5*, *GSDMB*, *GSDMD*, *NLRP7*, *NOD2*, *PYCARD*, *SCAF11*, and *NLRP6*—which effectively predicted the survival outcomes for patients with ccRCC.The results indicate that the identified genes might be useful prognostic markers for OS in ccRCC patients.

Furthermore, given its role in the tumor microenvironment, combining pyroptosis-related strategies with immunotherapy may offer a promising therapeutic strategy for ccRCC.

Availability of Data and Materials

The datasets that validate our findings are provided in the article. The datasets used and analyzed during the current study are available from the corresponding authors on reasonable request.

Author Contributions

GJL was responsible for performing the core bioinformatics analyses (including data mining, construction of the pyroptosis-related gene signature, and survival analysis), drafting the initial manuscript, and preparing figures. YRL contributed to data interpretation, and critical revision of the manuscript. WX was responsible for data curation and prepared figures. LFY was responsible for formal analysis and prepared figures. QX was responsible for the investigation and prepared figures. YL was responsible for methodology and prepared figures. YFL was responsible for software development and prepared figures. QL was responsible for project administration and prepared figures. CLL is the senior investigator who conceived the original research hypothesis, supervised the overall project direction, and coordinated collaborations. She also contributed to the experimental validation and prepared figures. TW designed and supervised the experimental validation work, contributed to data analysis, and has been responsible for manuscript revision and communication with the journal. All authors contributed to editorial changes in the manuscript. All authors read and approved the final manuscript. All authors have participated sufficiently in the work and agreed to be accountable for all aspects of the work.

Ethics Approval and Consent to Participate

All procedures involving human participants were performed in accordance with the ethical standards of the institutional and/or national research committee and with the Helsinki declaration (as revised in 2013). Informed consent was obtained from all individual participants included in the study. This study was approved by the Ethics Committees of The Fifth Affiliated Hospital, Southern Medical University (Approval Number: 2025-MNWK-K-002).

Acknowledgment

We thank Bullet Edits Limited for the linguistic editing and proofreading of the manuscript.

Funding

This work was funded by the Project of Administration of Traditional Chinese Medicine of Guangdong Province of China (20251263).

Conflicts of Interest

The authors declare that they have no known competing financial interests or personal relationships that could have appeared to influence the work reported in this paper.

Supplementary Material

Supplementary material associated with this article can be found, in the online version, at https://doi.org/10.31083/FBL51233.

References

[1] Siegel RL, Miller KD, Jemal A. Cancer statistics, 2020. CA: a Cancer Journal for Clinicians. 2020; 70: 7–30. https://doi.org/10.3322/caac.21590

[2] Vuong L, Kotecha RR, Voss MH, Hakimi AA. Tumor Microenvironment Dynamics in Clear-Cell Renal Cell Carcinoma. Cancer Discovery. 2019; 9: 1349–1357. https://doi.org/10.1158/2159-8290.CD-19-0499

[3] Linehan WM. Genetic basis of kidney cancer: role of genomics for the development of disease-based therapeutics. Genome Research. 2012; 22: 2089–2100. https://doi.org/10.1101/gr.131110.111

[4] Bella L, Zona S, Nestal de Moraes G, Lam EWF. FOXM1: A key oncofoetal transcription factor in health and disease. Seminars in Cancer Biology. 2014; 29: 32–39. https://doi.org/10.1016/j.semcancer.2014.07.008

[5] Bedke J, Gauler T, Grünwald V, Hegele A, Herrmann E, Hinz S, et al. Systemic therapy in metastatic renal cell carcinoma. World Journal of Urology. 2017; 35: 179–188. https://doi.org/10.1007/s00345-016-1868-5

[6] Choueiri TK, Fishman MN, Escudier B, McDermott DF, Drake CG, Kluger H, et al. Immunomodulatory Activity of Nivolumab in Metastatic Renal Cell Carcinoma. Clinical Cancer Research : an Official Journal of the American Association for Cancer Research. 2016; 22: 5461–5471. https://doi.org/10.1158/1078-0432.CCR-15-2839

[7] Loo V, Salgia M, Bergerot P, Philip EJ, Pal SK. First-Line Systemic Therapy for Metastatic Clear-Cell Renal Cell Carcinoma: Critical Appraisal of Emerging Options. Targeted Oncology. 2019; 14: 639–645. https://doi.org/10.1007/s11523-019-00676-y

[8] Hofmann F, Hwang EC, Lam TB, Bex A, Yuan Y, Marconi LS, et al. Targeted therapy for metastatic renal cell carcinoma. The Cochrane Database of Systematic Reviews. 2020; 10: CD012796. https://doi.org/10.1002/14651858.CD012796.pub2

[9] Choueiri TK, Motzer RJ. Systemic Therapy for Metastatic Renal-Cell Carcinoma. The New England Journal of Medicine. 2017; 376: 354–366. https://doi.org/10.1056/NEJMra1601333

[10] Rizzo A, Mollica V, Santoni M, Ricci AD, Rosellini M, Marchetti A, et al. Impact of Clinicopathological Features on Survival in Patients Treated with First-line Immune Checkpoint Inhibitors Plus Tyrosine Kinase Inhibitors for Renal Cell Carcinoma: A Meta-analysis of Randomized Clinical Trials. European Urology Focus. 2022; 8: 514–521. https://doi.org/10.1016/j.euf.2021.03.001

[11] Broz P, Pelegrín P, Shao F. The gasdermins, a protein family executing cell death and inflammation. Nature Reviews. Immunology. 2020; 20: 143–157. https://doi.org/10.1038/s41577-019-0228-2

[12] Liu X, Lieberman J. A Mechanistic Understanding of Pyroptosis: The Fiery Death Triggered by Invasive Infection. Advances in Immunology. 2017; 135: 81–117. https://doi.org/10.1016/bs.ai.2017.02.002

[13] Shi J, Zhao Y, Wang K, Shi X, Wang Y, Huang H, et al. Cleavage of GSDMD by inflammatory caspases determines pyroptotic cell death. Nature. 2015; 526: 660–665. https://doi.org/10.1038/nature15514
[14] Lin W, Chen Y, Wu B, Chen Y, Li Z. Identification of the pyroptosis-related prognostic gene signature and the associated regulation axis in lung adenocarcinoma. Cell Death Discovery. 2021; 7: 161. https://doi.org/10.1038/s41420-021-00557-2
[15] Deng M, Sun S, Zhao R, Guan R, Zhang Z, Li S, et al. The pyroptosis-related gene signature predicts prognosis and indicates immune activity in hepatocellular carcinoma. Molecular Medicine (Cambridge, Mass.). 2022; 28: 16. https://doi.org/10.1186/s10020-022-00445-0
[16] Lu X, Chen J, Lu Z, Zang H. Knockdown of *PAK1IP1* can Induce Pyroptosis to Inhibit the Progression of Hepatocellular Carcinoma. Frontiers in Bioscience (Landmark Edition). 2025; 30: 26654. https://doi.org/10.31083/fbl26654
[17] Wu J, Zhu Y, Luo M, Li L. Comprehensive Analysis of Pyroptosis-Related Genes and Tumor Microenvironment Infiltration Characterization in Breast Cancer. Frontiers in Immunology. 2021; 12: 748221. https://doi.org/10.3389/fimmu.2021.748221
[18] Shannon P, Markiel A, Ozier O, Baliga NS, Wang JT, Ramage D, et al. Cytoscape: a software environment for integrated models of biomolecular interaction networks. Genome Research. 2003; 13: 2498–2504. https://doi.org/10.1101/gr.1239303
[19] Bindea G, Mlecnik B, Tosolini M, Kirilovsky A, Waldner M, Obenauf AC, et al. Spatiotemporal dynamics of intratumoral immune cells reveal the immune landscape in human cancer. Immunity. 2013; 39: 782–795. https://doi.org/10.1016/j.immuni.2013.10.003
[20] Ru B, Wong CN, Tong Y, Zhong JY, Zhong SSW, Wu WC, et al. TISIDB: an integrated repository portal for tumor-immune system interactions. Bioinformatics (Oxford, England). 2019; 35: 4200–4202. https://doi.org/10.1093/bioinformatics/btz210
[21] Chen X, He WT, Hu L, Li J, Fang Y, Wang X, et al. Pyroptosis is driven by non-selective gasdermin-D pore and its morphology is different from MLKL channel-mediated necroptosis. Cell Research. 2016; 26: 1007–1020. https://doi.org/10.1038/cr.2016.100
[22] Fink SL, Cookson BT. Apoptosis, pyroptosis, and necrosis: mechanistic description of dead and dying eukaryotic cells. Infection and Immunity. 2005; 73: 1907–1916. https://doi.org/10.1128/IAI.73.4.1907-1916.2005
[23] Huang Y, Zhang Q, Lubas M, Yuan Y, Yalcin F, Efe IE, et al. Synergistic Toll-like Receptor 3/9 Signaling Affects Properties and Impairs Glioma-Promoting Activity of Microglia. The Journal of Neuroscience : the Official Journal of the Society for Neuroscience. 2020; 40: 6428–6443. https://doi.org/10.1523/JNEUROSCI.0666-20.2020
[24] Ruan J, Wang S, Wang J. Mechanism and regulation of pyroptosis-mediated in cancer cell death. Chemico-biological Interactions. 2020; 323: 109052. https://doi.org/10.1016/j.cbi.2020.109052
[25] Sarrio D, Colomo S, Moreno-Bueno G. Gasdermin-B (GSDMB) takes center stage in antibacterial defense, inflammatory diseases, and cancer. The FEBS journal. 2024; 291: 3060–3071. https://doi.org/10.1111/febs.17018
[26] Yang W, Hu X, Li X. Unveiling the role of gasdermin B in cancer and inflammatory disease: from molecular mechanisms to therapeutic strategies. PeerJ. 2025; 13: e19392. https://doi.org/10.7717/peerj.19392
[27] Sun L, Wang J, Li Y, Kang Y, Jiang Y, Zhang J, et al. Correlation of gasdermin B staining patterns with prognosis, progression, and immune response in colorectal cancer. BMC cancer. 2024; 24: 567. https://doi.org/10.1186/s12885-024-12326-2
[28] Hergueta-Redondo M, Sarrió D, Molina-Crespo Á, Megias D, Mota A, Rojo-Sebastian A. Gasdermin-B promotes invasion and metastasis in breast cancer cells. PLoS One. 2014; 9: e90099. https://doi.org/10.1371/journal.pone.0090099
[29] Molina-Crespo Á, Cadete A, Sarrio D, Gámez-Chiachio M, Martinez L, Chao K, et al. Intracellular Delivery of an Antibody Targeting Gasdermin-B Reduces HER2 Breast Cancer Aggressiveness. Clinical Cancer Research : an Official Journal of the American Association for Cancer Research. 2019; 25: 4846–4858. https://doi.org/10.1158/1078-0432.CCR-18-2381
[30] Saeki N, Usui T, Aoyagi K, Kim DH, Sato M, Mabuchi T, et al. Distinctive expression and function of four GSDM family genes (GSDMA-D) in normal and malignant upper gastrointestinal epithelium. Genes, Chromosomes & Cancer. 2009; 48: 261–271. https://doi.org/10.1002/gcc.20636
[31] Chao A, Huang HJ, Lai CH. Human papillomavirus research on the prevention, diagnosis, and prognosis of cervical cancer in Taiwan. Chang Gung Medical Journal. 2012; 35: 297–308. https://doi.org/10.4103/2319-4170.106141
[32] Topalian SL, Drake CG, Pardoll DM. Immune checkpoint blockade: a common denominator approach to cancer therapy. Cancer Cell. 2015; 27: 450–461. https://doi.org/10.1016/j.ccell.2015.03.001
[33] Fallarino F, Fields PE, Gajewski TF. B7-1 engagement of cytotoxic T lymphocyte antigen 4 inhibits T cell activation in the absence of CD28. The Journal of Experimental Medicine. 1998; 188: 205–210. https://doi.org/10.1084/jem.188.1.205
[34] Ross K, Jones RJ. Immune checkpoint inhibitors in renal cell carcinoma. Clinical Science (London, England : 1979). 2017; 131: 2627–2642. https://doi.org/10.1042/CS20160894
[35] Lin W, Zhang Y, Yang Y, Lin B, Zhu M, Xu J, et al. Anti-PD-1/Her2 Bispecific Antibody IBI315 Enhances the Treatment Effect of Her2-Positive Gastric Cancer through Gasdermin B-Cleavage Induced Pyroptosis. Advanced Science (Weinheim, Baden-Wurttemberg, Germany). 2023; 10: e2303908. https://doi.org/10.1002/advs.202303908
[36] Alishvandi A, Aram C, Shahrivar FF, Kesharwani P, Sahebkar A. Pyroptosis in cancer therapy: a double-edged sword for immune activation and tumor progression. Molecular Cancer. 2025; 24: 297. https://doi.org/10.1186/s12943-025-02506-4
[37] Chen J, Jiang R, Guan W, Cao Q, Tian Y, Dong K, et al. Novel model of pyroptosis-related molecular signatures for prognosis prediction of clear cell renal cell carcinoma patients. International Journal of Medical Sciences. 2024; 21: 496–507. https://doi.org/10.7150/ijms.88301
[38] Song X, Zhu Y, Geng W, Jiao J, Liu H, Chen R, et al. Spatial and single-cell transcriptomics reveal cellular heterogeneity and a novel cancer-promoting Treg cell subset in human clear-cell renal cell carcinoma. Journal for Immunotherapy of Cancer. 2025; 13: e010183. https://doi.org/10.1136/jitc-2024-010183
[39] Fu L, Bao J, Li J, Li Q, Lin H, Zhou Y, et al. Crosstalk of necroptosis and pyroptosis defines tumor microenvironment characterization and predicts prognosis in clear cell renal carcinoma. Frontiers in Immunology. 2022; 13: 1021935. https://doi.org/10.3389/fimmu.2022.1021935
[40] Lei K, Chen J, Deng Y, Peng Y, Zhai X, Ren X, et al. Cracking the code of cancer immunotherapy resistance: emerging roles of pyroptosis and necroptosis. Journal of Experimental & Clinical Cancer Research : CR. 2025; 44: 308. https://doi.org/10.1186/s13046-025-03569-3